Nanocavitation Around a Crack Tip in a Soft Nanocomposite: A Scanning Microbeam Small Angle X-Ray Scattering Study

Huan Zhang,[1] Arthur K. Scholz,[2,3] Jordan de Crevoisier,[1] Daniel Berghezan,[4] Theyencheri Narayanan,[5] Edward J. Kramer,[2,3,6] Costantino Creton[1]

[1]Laboratoire de Sciences et Ingénierie de la Matière Molle, ESPCI Paristech-CNRS-UPMC, 10 rue Vauquelin, 75005, Paris, France
[2]Materials Research Laboratory, University of California Santa Barbara, California 93106
[3]Department of Materials, University of California Santa Barbara, California 93106
[4]Michelin, CERL Ladoux, F-63040 Clermont Ferrand, France
[5]ESRF, 71, Avenue des Martyrs, 38043 Grenoble Cedex 9, France
[6]Department of Chemical Engineering, University of California Santa Barbara, California 83106
Correspondence to: H. Zhang (E-mail: mindcontrol1569@gmail.com) or C. Creton (E-mail: Costantino.Creton@espci.fr) or E. J. Kramer (E-mail: edkramer@mrl.ucsb.edu)

Received 29 October 2014; accepted 18 November 2014; published online 24 December 2014
DOI: 10.1002/polb.23651

ABSTRACT: We explore nanocavitation around the crack tip region in a styrene-butadiene random copolymer filled with typical carbon black (CB) particles used in the rubber industry for toughening the rubber. Using quasistatic loading conditions and a highly collimated X-ray microbeam scanned around the crack tip, we demonstrate the existence of a damage zone consisting of nanovoids in a filled elastomer matrix. The existence of voids near the crack tip is demonstrated by a significant increase of the scattering invariant Q/Q_0 in front of both fatigued and fresh cracks. The size of the zone where cavities are present critically depends on the macroscopic strain ε_m, the loading history, and the maximum energy release rate G applied to accommodate the crack. Our findings show that nanovoiding occurs before fracture in typical CB-filled elastomers and that realistic crack propagation models for such elastomers should take into account a certain level of compressibility near the crack tip. © 2014 Wiley Periodicals, Inc. J. Polym. Sci., Part B: Polym. Phys. **2015**, *53*, 422–429

KEYWORDS: elastomers; fracture; nanocomposites; SAXS

INTRODUCTION Filled elastomers are unarguably an important class of structural materials and have found lasting successes in the tire industry and other cutting edge technological applications such as oil exploration[1] and conductive adhesives.[2] However, understanding their failure mechanisms to be able to predict the lifetime of the products remains an unsolved problem and becomes an emergency due to the deficiency of natural oil-based resources. A robust materials design to prevent fracture requires the local strain energy around a crack tip to be effectively dissipated into a large volume of process zone.[3,4] The first step therefore is to gain a deep insight into the energy dissipation mechanisms in the process zone, from the molecular to the macroscopic level.[5,6] So far, several intrinsic toughening mechanisms have been observed in other materials such as viscoplastic flow in gels,[7,8] microcracking and crazing in ceramics[9] and polymers,[10–14] and shear banding in metallic alloys and polymers,[15,16] to name a few. While in most classes of materials such as metals and glassy and semicrystalline polymers the presence of a clear yield stress makes the dissipative mechanisms in front of the crack readily observable by electron microscopy, this is not the case with elastomers. Electron microscopy observations at the crack tip under load are nearly impossible because of beam damage and relaxation. Furthermore, the absence of a well-defined yield stress means that the type of highly localized plastic deformation observed in glassy or semi-crystalline polymers at the crack tip[17–20] is not observed. In filled and unfilled elastomeric materials, the only toughening mechanism reported is strain induced crystallization[21–24] which has been detected at the crack tip in natural rubber by wide-angle X-ray scattering.

The last decade has witnessed significant advances in the *in situ* investigation of the morphology and the strain field at the 10–100 μm length scale around the crack tip of

Conflict of Interest: The authors declare no competing financial interest.

Additional Supporting Information may be found in the online version of this article.

elastomers by varied techniques.[22–27] Le Cam et al. observed ligaments of a few hundred microns in diameter at the very tip of a crack in a carbon black (CB) filled natural rubber by scanning electron microscope.[25] The presence of similar fibrillar structures were reported in other filler-gum systems.[28] To explain the presence of ligaments on the crack front, one may imagine that cavities are nucleated in the process zone and further coalesce to form microcracks,[29] which are likely the precursors of the observed ligaments.[22,25,27] This hypothesis is consistent with the presence of multiaxial stresses ahead of the crack tip in thick samples of strain–hardening elastomers.[30,31] However, limited by the spatial resolution of the previous techniques, cavitation at the submicron length scale near the crack tip in filled elastomers has never been explored and demonstrated to date.

Recently, we have developed a methodology using real time small angle X-ray scattering (SAXS) and the measurement of the scattering invariant Q[32] to probe the existence of nanocavities in filled elastomers.[33–35] In a CB filled styrene-butadiene rubber (SBR) containing 15–20 vol % of CB nanoparticles, a sharp increase of the scattering invariant above a critical (macroscopic) strain ε_{Cav} and/or a critical (macroscopic) stress σ_{Cav} was observed in uniaxial loading. This increase in Q was attributed to the following mechanism: the rearrangement of the filler aggregates under strain generates significant triaxial stresses in locally confined regions between CB agglomerates and these local triaxial stresses then drive nanocavitation, which is detected by SAXS. For the experimental system investigated, the average size of these nanovoids was in the 20–40 nm range and decreased with strain. We systematically investigated the effects of filler volume fraction, cross linking density,[33] and loading history[34] on ε_{Cav} and σ_{Cav} as well as on the size and shape of nanovoids. A very similar behavior was observed in a natural rubber matrix filled with the same type of CB.[35] These results have also been quantitatively confirmed by macroscopic volume variation tests[33–36] and provide a mechanistic proof of earlier reports of volume change of filled elastomers in uniaxial tension.[37,38]

Such nanocavities and the associated change in volume in uniaxial extension is unusual for rubbers and was only observed for large values of extension λ. In the case of the crack tip, the high stress strongly promotes the nucleation of nanovoids in the tip region, which may further lead to the ligaments structure revealed during crack propagation. However, near a crack tip, the presumed cavitation region inside the process zone is likely to be strongly localized ($<$200 μm).[26] A successful structural investigation around the crack tip hence requires access to both smaller beam size ($<$50 μm) and a low q range to detect large objects ($\sim$100 nm).

Several WAXS investigations of the crack tip have been carried out before on filled elastomers with a small beam size. Trabelsi et al., and Rublon et al. investigated the region near the crack tip of a filled natural rubber by WAXS with a 200 μm diameter beam,[21,24] More recently Bruning et al. also investigated the region near the crack tip by WAXS of a natural rubber in a fatigue experiment with a much smaller beam (30 $\times$ 20 μm) but the fast acquisition rate of the dynamic experiment and the moving sample limited the spatial resolution to around 100 μm.[23] SAXS has been extensively used to investigate the damage mechanisms of glassy polymers[14,39–41] but rarely used at the crack tip. Lorenz-Haas and coworkers tried to map the region near the crack tip of a PMMA sample and only achieved a limited resolution with a 300 μm diameter beam and Bruning et al.[23] used the same setup as for WAXS for a preliminary investigation by USAXS at the crack tip. They showed the existence of a small (100 $\times$ 500 μm) cavitated zone in front of the crack for highly filled natural rubber able to strain crystallize.

Thanks to the development of highly collimated micro-X-ray beams at the European Synchrotron Radiation Facility (ESRF),[42] it is now possible to explore more extensively and systematically the crack tip region, at least statically, with a spatial resolution of the order of 20–30 μm. This has made this tool ideal for the investigation of the local occurrence of nanovoids in filled elastomers. Herein, for the first time, we show conclusively that a damaged zone containing nanovoids exists around the crack tip in a CB highly filled noncrystallizing SBR elastomer under quasistatic loading. The effects of macroscopic strain and loading history on the volume fraction of the cavities are discussed.

EXPERIMENTAL

Sample Preparation

A SBR copolymer ($M_n = 120$ kg mol^{-1}, $M_w/M_n = 1.94$, $T_g = -48$ °C, 0.15 mol fraction of styrene) was mixed with CB N347. This type of CB is typically used in tires and has a very high specific area and individual particle sizes of the order of 30 nm. The volume fraction of the filler was fixed at 23.9% (60 phr, parts of weight per hundred parts of rubber), which exhibited the most pronounced cavitation under uniaxial loading in our previous study.[33,34] The crosslinking system was based on sulfur and *n*-cyclohexyl-2-benzothiazyl-sulfenamide. The antioxidant N-(1,3-dimethylbutyl)-*N*′-phenyl-p-phenylenediamine 6PPD (1,9 phr), the vulcanization activators stearic acid (2 phr) and zinc oxide (2.5 phr) were used for curing. The sample was cured at 150 °C for 15 min. The resulting crosslinking density was estimated to be 7.7 $\times$ 10^{-5} mol cm^{-3} by swelling experiments analyzed using the Flory-Rehner equation[43] assuming that the filler cannot swell. Uncross-linked samples were then molded into samples with a pure shear geometry (Supporting Information Fig. S13), that is, strips of length $L_0 = 35$ mm, height $H_0 = 6.0$ mm, and thickness $T_0 = 0.8$ mm.

Crack Accommodation

"Crack accommodation" is typically used to obtain a crack tip shape, which is independent of the initial conditions. Unnotched samples were first strained for 10,000 cycles from zero strain to a maximum tensile strain of 30% (defined as $\varepsilon = \Delta H/H_0$ where ΔH is the change of height and H_0 is the initial height) at a frequency $f = 10$ Hz to avoid the

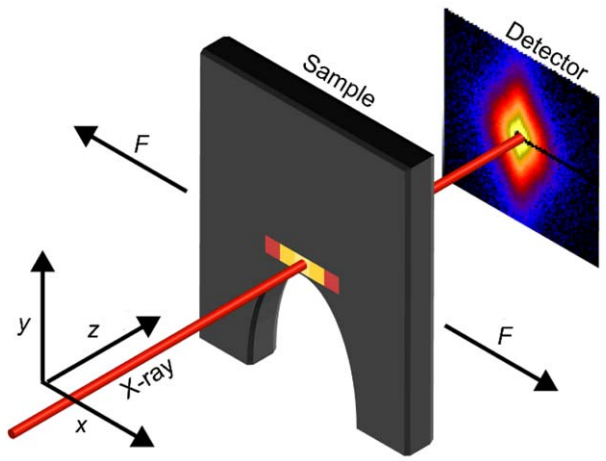

FIGURE 1 The setup of the scanning experiment: *x*, tensile direction; *y*, crack propagation direction; *z*, beam direction. [Color figure can be viewed in the online issue, which is available at wileyonlinelibrary.com.]

stress-softening effect (Mullins effect).[26] An edge crack (10 mm) was then cut with a razor blade along the length direction. The notched specimens were subjected to 20000 cycles ($f = 16$ Hz) to a maximum accommodation strain ε_a ($\varepsilon_a < 30\%$) that corresponds to various maximum values of the energy release rate G. After typically 5000 cycles, the crack propagation velocity and crack tip shape remain nearly constant.[28] The samples will be referred to as **G700** ($\varepsilon_m = 7.7\%$), **G1500** ($\varepsilon_m = 12\%$), and **G3000** ($\varepsilon_m = 19.2\%$), in which the number denotes the maximum energy release rate G (J m^{-2}) applied to the cracked samples during the cycling. Fatigued samples were stored at -20 °C to prevent physical aging until one hour before the experiment at the beamline. Other specimens with fresh cracks, made with a razor blade, were also prepared. The idea to compare the damage in front of fresh cracks and of accommodated cracks is to assess whether the accommodation, in addition of changing the crack shape has also damaged the crack tip zone in a way that favors the nucleation of cavities.

SAXS Measurements

The SAXS experiments were performed at beamline ID02 at ESRF (Grenoble, France). The wave length λ of the X-ray was 0.099 nm and the sample to detector distance was 10 m. The scattering vector q is defined as $q = 4\pi/\lambda \sin(\theta)$ where 2θ is the scattering angle and the accessible q range was between 0.006 and 0.5 nm^{-1} in this work. A sketch of the scattering experiments is drawn in Figure 1 and the coordinates in this study are defined as: *x*, tensile direction; *y*, crack direction; *z*, beam direction. The specimen was stretched to the desired macroscopic strain ε_m ($\varepsilon_m = \Delta H/H_0$ where ΔH is the change of height and H_0 is the initial height) with a 200 N, Deben mini tensile tester and held still during data acquisition.

A scan of the transmitted beam intensity *IC*2 in the *x*-*y* plane (Fig. 1) was first performed before the actual experiment to determine the position of the crack tip. It should be noted that the diameter of the beam used in this study was 20 and 30 μm thus it was difficult to get the precise position of the crack tip (within a few microns). An exposure with a *y* coordinate 4 mm in front of the crack tip (in the *x*-*y* plane) was first taken as a reference. The acquisition time was extremely short, 0.02 s, to minimize radiation damages (if there were any) on the samples. Two types of scanning experiments were then followed:

A: The beam size used was 20 × 20 μm. A continuous scan was performed around the crack tip. The scanning area was from -160 μm (left of the crack tip) to 120 μm (right of the crack tip) along the tensile direction *x* and from -40 μm (in the crack) to 140 μm (in front of the crack tip) along the crack direction *y*. The step length was 20 μm in both directions therefore there was no overlapping of the scattering patterns. This procedure was only applied to a fresh crack to obtain a full 2D scan of the crack tip region. **B:** The beam size used was 30 × 30 μm. Three *y*-scans at a fixed *x* coordinate relative to the crack tip were performed followed by three *x*-scans at fixed *y* coordinate. The scan step was 12.5 μm (smaller than the size of the beam therefore the scattering patterns were partially overlapped). This procedure was applied to all other experiments.

DATA REDUCTION

The details on the data reduction can be found in the Supporting Information as well as in previous publications.[33–35]

Correction of the Scattering Intensity

The incident beam intensity *IC*1 and the transmitted beam intensity *IC*2 were measured from two different apparatus so a correlation factor is defined as: $R = (IC1_{air}/IC2_{air})$. The in-house data acquisition system at ID-02 automatically carried out most of the data reduction (see Supporting Information for details) and gave the corrected scattering intensity $I_{img}(q)$.

Calculation of the Scattering Invariant

To calculate the scattering invariant Q_{img}, I_{img} (q) was integrated under a cylindrical symmetry assumption (along the tensile direction *x*):

$$Q_{img} = \frac{1}{2}\int_{-\infty}^{+\infty}\int_{0}^{\infty} I_{img}(q_x, q_{yz})\, q_{yz}\, dq_x\, dq_{yz} \quad (1)$$

At the edges of the crack, some of the streaks (scattering patterns from nanovoids) were slightly rotated relative to the tensile axis (Supporting Information Fig. S4) and therefore deviated from the cylindrical symmetry assumption. We demonstrated that the tilting of the streaks had a negligible effect on the calculation of Q_{img} (see Supporting Information). The integration limits cannot be zero and infinity since the data is collected over a limited range of q values. At low q, we neglect the scattering, which means assuming that there is a negligible volume fraction of large cavities. At large

q, A Porod tail was applied and the details have been published previously.[34]

The thickness of the sample affects the absorption and the scattering volume of the sample during the SAXS test. The former effect is already corrected by the in-house data acquisition system at ID-02 (see Equation S1 in Supporting Information). The latter effect is considered here: Q_{img} was normalized to the value of Q at the reference position (denoted as Q_{img_ref}) to get the normalized scattering invariant Q/Q_0.

$$\frac{Q}{Q_0} = \frac{Q_{img}}{Q_{img_{ref}}} \frac{t_{ref}}{t} \quad (2)$$

where t, t_{ref} are the thickness near the crack and at the reference position, respectively. The right term in eq 2 is to correct for the thickness change due to straining of the sample.

The calculation of Q/Q_0 is very sensitive to the precision of the photodiode reading IC2. In previous work carried out in uniaxial tension, the value of t_{ref}/t could be obtained from the value of R and the ratio of $IC2$ to $IC1$. However, in this work because of the small beam size and short acquisition time, the ratio $IC2/IC1$ was less reliable ($IC1$ is located before the last collimation element and any small vibration in the surroundings could perturb the ratio though $IC2$ photodiode still recorded the correct transmitted intensity) and could not be reliably used to measure thickness. We hence developed a new algorithm to calculate the value of t_{ref}/t (see details in Supporting Information). It should be noted that this new algorithm can underestimate the value of Q/Q_0 very close to the crack tip.

Calculation of the Void Volume Fraction

The void volume fraction ϕ_{void} was evaluated based on a previously developed three-phase model.[33–35]

$$\frac{Q}{Q_0} = 1 + \left[\frac{\phi_{SBR}\rho_{SBR}^2 + \phi_{CB}\rho_{CB}^2}{\phi_{SBR}\phi_{CB}(\rho_{SBR} - \rho_{CB})^2} - 1 \right] \phi_{void} \quad (3)$$

where ρ_{SBR} (8.756×10^{10} cm^{-2}) and ρ_{CB} (15.26×10^{10} cm^{-2}) are the X-ray scattering length density of the SBR matrix and of the CB filler particles, respectively. ϕ_{SBR} and ϕ_{CB} (23.8%) are the volume fraction of the polymer matrix and filler particles, respectively.

Plotting Q/Q_0 in the x-y Plane

For Procedure **A**, the obtained Q/Q_0 values were directly plotted without further treatment. For Procedure **B**, the scattered data points were interpolated onto a mesh grid using Matlab program to obtain matrixed data of Q/Q_0.

RESULTS AND DISCUSSION

Fresh Crack

In a first set of experiments, a specimen with a fresh notch was stretched to different values of ε_m and the crack tip region was scanned with a beam size of 20×20 μm. In Figure 2, the normalized scattering invariant Q/Q_0 in the x-y plane at $\varepsilon_m = 90\%$ is shown. As expected, Q/Q_0 was around 1 (i.e., no additional scatterers) in the bulk region far from the crack tip, but then significantly increased to 1.8 as the distance along y toward the crack tip decreased, indicating the appearance of additional scattering objects, that is, nanovoids. Figure 2 also gives us an estimate of the size of the zone where cavitation was observed at $\varepsilon_m = 90\%$. The width W along the tensile direction (x) was at least larger than 300 μm since the values of Q/Q_0 close to the crack tip at $x = -150$ and 125 μm (green color, around 1.6) were still well above 1. Along the other direction, the height H of the cavitation zone in the crack direction (y) was clearly <100 μm. Thus, the shape of the cavitation zone was highly elongated in the tensile direction at $\varepsilon_m = 90\%$. Moreover, the contour line of the cavitation zone exhibited a concave-downwards shape, which resemble the shape of the crack tip.

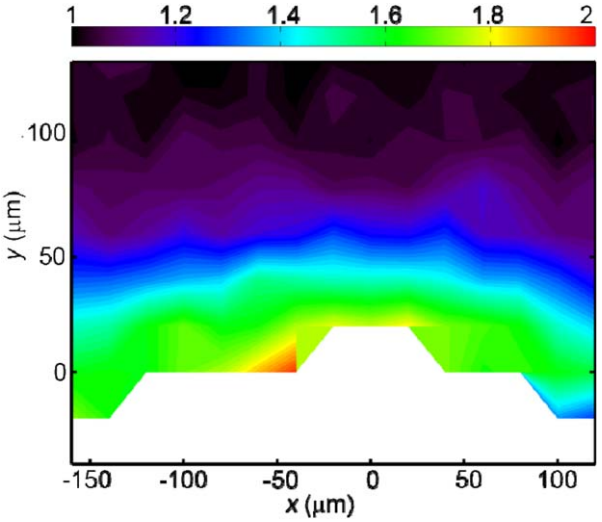

FIGURE 2 Color-coded map of the normalized scattering invariant Q/Q_0 in the x-y plane in front of the crack tip for a specimen with a fresh crack with a sample strained at $\varepsilon_m = 90\%$. The crack tip is positioned at $x = 0$ and $y = 0$. [Color figure can be viewed in the online issue, which is available at wileyonlinelibrary.com.]

Selected SAXS patterns are shown in Figure 3 (See Supporting Information Fig. S4 for all 300 SAXS patterns for this scan). Far from the crack tip, a faint butterfly shape was present close to the beamstop, which was due to the reorganization of the filler aggregates.[34,44] Just 20 μm in front of the crack tip, a bright streak developed perpendicular to the stretching direction, indicating the presence of nanovoids highly oriented along the tensile axis. In the neighboring region very close to the edge of the crack tip, some of the cavitation streaks were slightly tilted from the equator (Supporting Information Fig. S4), implying a distributed orientation of nanovoids. This slight deviation from the cylindrical symmetry (rotated streaks) was found to have no influence on the calculation of the scattering invariant Q/Q_0 (Supporting Information Fig. S1). These results are consistent with previous findings under uniaxial loading.[33–35]

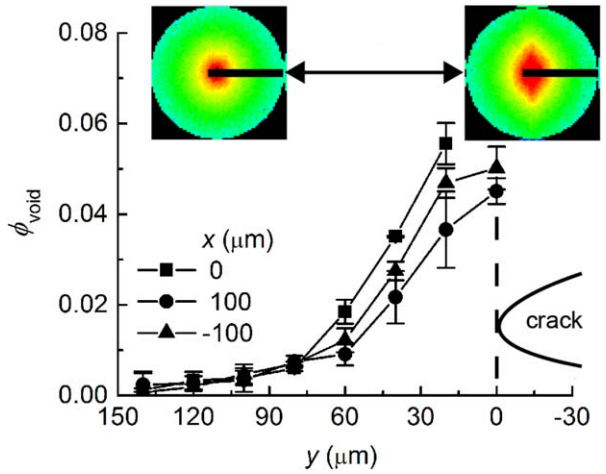

FIGURE 3 Void volume fraction ϕ_{void} along the crack plane y towards the tip at fixed x values indicated in the legend for a fresh sample strained at $\varepsilon_m = 90\%$. The error bars are the average from neighboring pixels. The insets are typical scattering patterns (logarithmic scale) 150 μm from the crack tip (left) and 20 μm (right) from the crack tip. The double-headed arrow indicates the tensile direction for the patterns and the dashed line indicates the position of the crack tip (for the main graph). x is the tensile direction and y is the crack propagation direction. [Color figure can be viewed in the online issue, which is available at wileyonlinelibrary.com.]

The values of ϕ_{void} were calculated using eq 3 and are plotted against y in Figure 3. It should be noted that we may have underestimated ϕ_{void} very close to the crack tip, at values of local strain exceeding 300% (see Supporting Information for details). As y approached the crack tip from the bulk, ϕ_{void} started to increase at $y = 100$ μm and finally reached 5.6% at $y = 20$ μm. This result confirmed our previous observation that the thickness H of the zone where cavitation is detected in the y direction was <100 μm (Fig. 2). We further notice that this value of void volume fraction would be observed for a macroscopic strain of about 300% in uniaxial tension for the same materials.[33] Therefore the local strain around the crack tip was roughly three times that of ε_m (90%), consistent with previous measurements of the strain field near crack tip by digital image correlation.[26] When the beam was partially or completely in the crack, ϕ_{void} became meaningless and the data points where part of the beam was inside the crack are therefore not shown. The values of ϕ_{void} at other two positions ($x = \pm$ 100 μm) are also depicted in Figure 3. They were comparable with the ones at $x = 0$ μm, showing that the cavitated zone was indeed rather homogeneous and elongated in the tensile direction x.

Fatigued Crack

In practice, catastrophic failure of rubber products often starts from preexisting fatigued cracks so we then directed our effort to investigate nanocavitation in notched samples that were previously submitted to cyclic loading. These investigations were made with a beam size of 30 × 30 μm.

Effect of Macroscopic Strain ε_m

In Figure 4, ϕ_{void} of a notched sample **G3000** previously submitted to 20,000 loading cycles (Supporting Information) is plotted as a function of y for varying values of macroscopic strain ε_m. At $\varepsilon_m = 30\%$, ϕ_{void} fluctuated around zero and the related 2D mapping of Q/Q_o in the x-y plane [Fig. 5(a), see also Supporting Information Fig. S6–S8] was featureless at first glance. However, careful inspection of the SAXS patterns near the tip revealed a similar streak formation (therefore strong scattering) in the low q range as that shown in Figure 3. However, the scattering intensity abruptly and unexpectedly dropped at high q range. We then deduced that the cavitation zone was still present in the process zone directly ahead of the crack tip for small ε_m. However, its height H was smaller than the beam size so that the spot was partially off the sample in the crack. The increase of Q due to the presence of nanovoids was then compensated by a great loss of scattering objects. As ε_m was further increased, the cavitation zone significantly increased in size in both x and y directions and the maximum value of ϕ_{void} near the tip increased as well. For example, at $\varepsilon_m = 60\%$, similar 2D patterns of Q/Q_o as fresh samples at $\varepsilon_m = 90\%$ were observed in the x-y plane [Fig. 5(b)] and the value of ϕ_{void} in the tip region reached 6.0 % (Fig. 4). At $\varepsilon_m = 90\%$, the crack even became unstable and propagated about 30 μm in the damaged zone along the y axis. After the crack stopped, the scanning revealed a maximum value of ϕ_{void} of about 9% in the tip region. Collectively, the above results imply that the size of the cavitation zone, especially H, depends critically as expected, on the applied macroscopic strain ε_m. Moreover, if compared at the same $\varepsilon_m = 90\%$ (Figs. 3 and 4), the severely fatigued sample **G3000** exhibited a significantly larger cavitation zone as well as higher value of ϕ_{void} than the sample with a fresh crack, suggesting that the

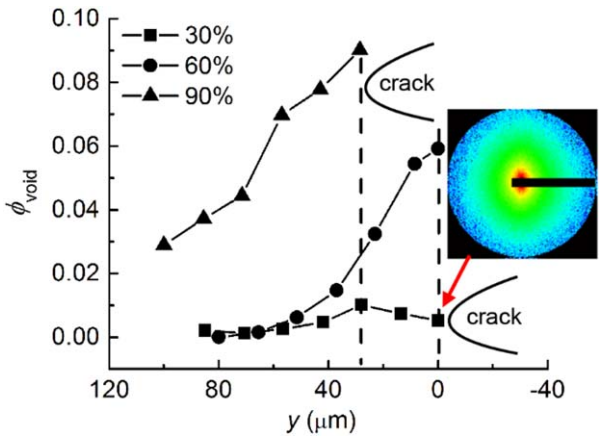

FIGURE 4 Void volume fraction ϕ_{void} of a fatigued sample **G3000** as a function of the distance y towards the tip ($x = 0$ μm) at varied macroscopic strain ε_m indicated in the legend. The dashed lines are the indication of the crack tip. A selected SAXS pattern near the crack tip at $\varepsilon_m = 30\%$ is shown. The stretching axis is horizontal for the SAXS pattern. [Color figure can be viewed in the online issue, which is available at wileyonlinelibrary.com.]

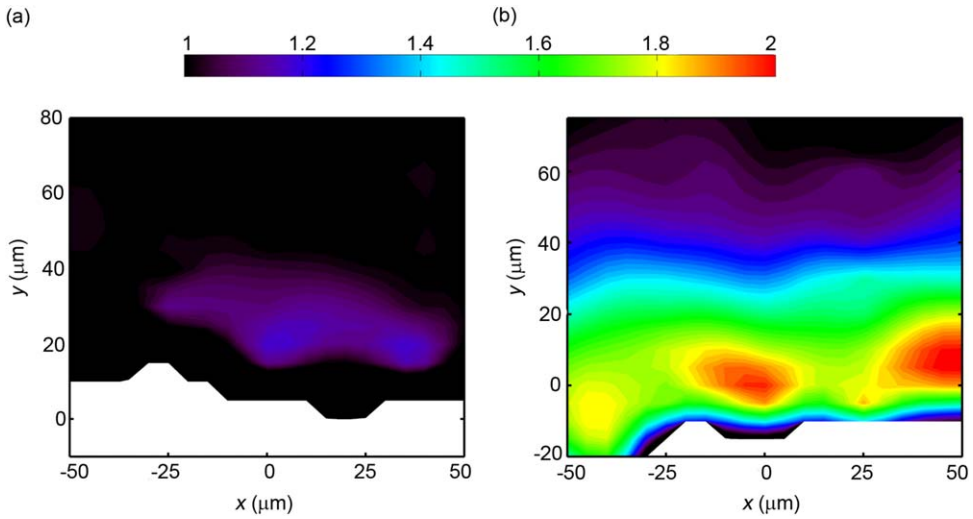

FIGURE 5 2D mapping of Q/Q_0 for a fatigued sample **G3000** in the *x*-*y* plane at (a) $\varepsilon_m = 30\%$ and (b) $\varepsilon_m = 60\%$. [Color figure can be viewed in the online issue, which is available at wileyonlinelibrary.com.]

repeated cycling created sufficient material damage in front of the crack to affect cavitation It should be noted that the difference in crack tip voiding observed between the fresh sample (Fig. 3) and the fatigued sample (Fig. 4) at the same value of ε_{max} is much larger than the expected variation from sample to sample for noncrystallizing SBR where the crack tip shapes are fairly reproducible and independent of the applied G value. Therefore, the damage produced during the cycling at $G = 3000$ J/m^2 ($\varepsilon_{max} = 19\%$) has damaged the material near the crack tip to the point that our loading at a much higher value of strain ($\varepsilon_m = 90\%$) created much more voiding than the equivalent strain on a sample that is not damaged by the cycling.

Effect of Loading History

In previous work on the same material,[34] we observed a very peculiar behavior under cyclic uniaxial loading. The nanovoids only formed during the first loading and they never reopened upon successive loadings once closed during unloading by surface tension. Moreover, new nanovoids only appeared when the strain exceeded the maximum stretch (or stress) attained in previous loadings. We tried to repeat a similar experiment near the crack tip where, for incompressible rubbers the stress field varies from uniaxial (at the crack tip)[45] to pure shear, that is, biaxial (away from the crack tip).[31,45] A **G3000** specimen was first stretched to $\varepsilon_m = 60\%$. Q/Q_0 in the *x*-*y* plane (Supporting Information Fig. S9) revealed a severely cavitated zone around the crack tip with a maximum value of ϕ_{void} around 6%. Then the specimen was unloaded until the load reached zero and immediately stretched again to $\varepsilon_m = 60\%$. Because the sample position was identical in the beam we could check that this reopening (second loading) did not lead to a propagation of the crack within our resolution (30×30 μm).

The cavitation zone was still there in the second loading (Fig. 6 and see Supporting Information Fig. S9) with a decreased size of cavitation zone and a drop of the maximum value of ϕ_{void} to 4%. We therefore infer that roughly two-thirds of the nanovoids could still reopen in the successive loadings in the crack tip region whereas this ratio was zero under pure uniaxial loading of a fresh sample.[34]

In previous work, this absence of reopening of the nanovoids in uniaxial loading was interpreted to be due to the rearrangement of the filler aggregates and consequently to the release of local confinements in the tensile direction.[34] However, such scenario may not be correct in the process zone as the local stress field is more complex with significant macroscopic biaxiality or triaxiality of the stress. In such a loading situation, the rearrangement of the filler aggregates may be different from the case of uniaxial tension, not sufficiently removing the regions of local confinement between fillers and resulting in a reopening of the nanovoids (which

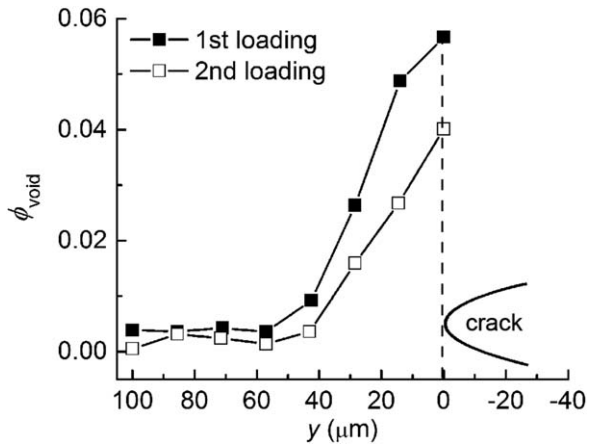

FIGURE 6 ϕ_{void} of a fatigued sample **G3000** as a function of the distance *y* toward the tip ($x = 0$ μm) at two different loading cycles ($\varepsilon_m = 60\%$) indicated in the legend. The dashed line indicates the crack tip.

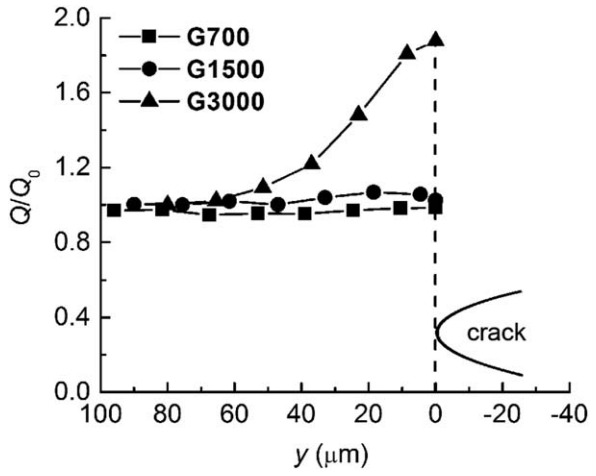

FIGURE 7 Q/Q_0 of samples fatigued under different maximum energy release rate G indicated in the legend ($x = 0$ μm, $\varepsilon_m = 60\%$).

must lead to weak spots) in the second loadings. In addition, we carried out this experiment with a sample submitted to 20,000 cycles at $\varepsilon_m = 19\%$ which may have damaged the crack tip region relative to the fresh sample.

Effect of Energy Release Rate G

In the last section, we qualitatively studied the effect of fatigue conditions on the size of the cavitation zone. Notched samples were first fatigued offline for 20,000 cycles under different applied G (**G700**, **G1500**, and **G3000**). They were then stretched to the same $\varepsilon_m = 60\%$ in the beam and the values of Q/Q_0 along the y direction at $x = 0$ μm is illustrated in Figure 7. Under mild fatigue conditions ($G = 700$, 1500 J m^{-2}), Q/Q_0 again fluctuated around 1 (Fig. 7 and Supporting Information Fig. S10) but the characteristic streak patterns near the crack tip were discernible. Hence, the cavitation zones may be still present in the tip region in **G700** and **G1500** specimens at $\varepsilon_m = 60\%$, but the size of the cavitation zone was again smaller than the beam size (30 μm), similar to the case of **G3000** at $\varepsilon_m = 30\%$ (Fig. 4). In contrast, **G3000** always resulted in the largest area of the cavitation zone as well as the highest value of ϕ_{void} under the same ε_m. We therefore conclude that the size of the cavitation zone also depended on the value of G experienced by the crack during the fatigue conditions.

The effect of G on the cavitation around the crack tip can be interpreted as a result of the (macroscopic) accommodation strain ε_a applied to the crack (see Experimental Section). For **G700** and **G1500**, ε_a was so small that the local strain around the crack tip may be below or just above the critical cavitation strain ε_{Cav} (about 160% under uniaxial loading for this composition[33]), resulting in a very narrow cavitation zone. When the beam (30 μm for fatigued samples) illuminated this region, part of the microbeam was already off the sample. Therefore, even if the features of nanovoids were visible on the 2D SAXS patterns, the corresponding values of Q/Q_0 never increased above 1. As for **G3000**, the local strain associated with ε_a was much higher than ε_{Cav}. As a consequence, a sufficiently large cavitation zone (> beam size) was created during crack accommodation and could be easily detected by the X-ray beam. To confirm our hypothesis, a higher value of ε_m (90%) was applied to **G700** to enlarge the cavitation zone. Indeed, abrupt increases of Q/Q_0 and streak SAXS patterns were observed in these specimens (Supporting Information Figs. S11 and S12). These results show that cavities do indeed form in front of crack tips propagating in fatigue conditions in elastomers filled with so-called reinforcing CB nanoparticles (N347). More generally, the threshold of appearance of the nanocavitation mechanism in uniaxial extension has been shown to depend on the filler volume fraction[33,34] and certainly on the nature of the filler.[35,46,47] At the crack tip, this will result in a different size of the cavitated zone for the same macroscopic loading conditions. However, our evidence strongly suggests that elastomers filled with nanoparticles will form nanocavities in a region close to the crack tip and any physically based damage models should take this feature into account. Knowing that the eventual fracture occurs by the failure of nearly independent micron size fibrils,[27,28] one can propose that the nanocavities release the incompressibility constraint and that nanocavity coalescence leads then to a highly anisotropic fibrillar zone. The failure criterion of this fibrillar zone has been discussed by Mzabi et al.[26] and appears to be related to the density of locally stored elastic energy in the fibrillar zone, and to its size.

CONCLUSIONS

To conclude, we harnessed microfocus X-ray beam to investigate the nucleation of nanocavities around a crack tip in a CB filled SBR. A damage zone in the form of nanocavities around the crack tip was for the first time confirmed in notched (either fatigued or freshly cut) non-crystallizing SBR specimens. The shape of the cavitation zone was highly anisotropic (narrow along the crack direction). Its size as well as the maximum void volume fraction were critically dependent on the macroscopic strain, the number of loading cycles, and the maximum energy release rate imposed to the crack during the accommodation. Under identical loading conditions, samples with fatigued cracks showed a stronger tendency to cavitate than those with fresh cracks. These findings shed some light on how the fibrillar zones observed at crack tips in filled elastomers can form from an initially homogeneous material and how fatigue loading can increase the density of cavities and the size of the zone where they appear.

ACKNOWLEDGMENT

The work was supported by the French ANR Project AMUFISE, (MATETPRO 08-320101). A. K. S and E. J. K were supported by the Institute for Multiscale Materials Studies at UCSB, collaboration with Los Alamos National Laboratory. The scattering experiments were performed at the ID02 beamline at the European Synchrotron Radiation Facility (ESRF), Grenoble, France.

REFERENCES AND NOTES

1 M. Endo, T. Noguchi, M. Ito, K. Takeuchi, T. Hayashi, Y. A. Kim, T. Wanibuchi, H. Jinnai, M. Terrones, M. S. Dresselhaus, *Adv. Funct. Mater.* **2008**, *18*, 3403–3409.

2 R. Ma, S. Kwon, Q. Zheng, H. Y. Kwon, J. I. Kim, H. R. Choi, S. Baik, *Adv. Mater.* **2012**, *24*, 3344–3349.

3 E. Ducrot, Y. Chen, M. Bulters, R. P. Sijbesma, C. Creton, *Science* **2014**, *344*, 186–189.

4 H. Peterlik, P. Roschger, K. Klaushofer, P. Fratzl, *Nat. Mater.* **2006**, *5*, 52–55.

5 T. Giesa, N. M. Pugno, J. Y. Wong, D. L. Kaplan, M. J. Buehler, *Adv. Mater.* **2014**, *26*, 412–417.

6 R. O. Ritchie, *Nat. Mater.* **2011**, *10*, 817–822.

7 T. Baumberger, C. Caroli, D. Martina, *Eur. Phys. J. E* **2006**, *21*, 81–89.

8 J.-Y. Sun, X. Zhao, W. R. K. Illeperuma, O. Chaudhuri, K. H. Oh, D. J. Mooney, J. J. Vlassak, Z. Suo, *Nature* **2012**, *489*, 133–136.

9 A. Hamilton, C. Hall, *J. Phys. D: Appl. Phys.* **2013**, 46.

10 E. Kramer, *J. Polym. Eng. Sci.* **1984**, *24*, 761–769.

11 P. J. Mills, E. J. Kramer, H. R. Brown, *J. Mater. Sci.* **1985**, *20*, 4413–4420.

12 A. M. Donald, E. J. Kramer, *J. Mater. Sci.* **1981**, *16*, 2967–2976.

13 H. R. Brown, E. J. Kramer, R. A. Bubeck, *J. Polym. Sci. Part B: Polym. Phys.* **1987**, *25*, 1765–1778.

14 H. R. Brown, E. J. Kramer, *J. Macromol. Sci Phys.* **1981**, *B19*, 487–522.

15 D. C. Hofmann, J.-Y. Suh, A. Wiest, G. Duan, M.-L. Lind, M. D. Demetriou, W. L. Johnson, *Nature* **2008**, *451*, 1085–U1083.

16 A. Donald, E. Kramer, *J. Mater. Sci.* **1981**, *16*, 2967–2976.

17 P. P. Cortet, S. Santucci, L. Vanel, S. Ciliberto, *Europhys. Lett.* **2005**, *71*, 242.

18 C. J. G. Plummer, *Adv. Polym. Sci.* **2004**, *169*, 75–119.

19 C.J. G. Plummer, P. Béguelin, H.-H. Kausch, *Colloids Surf. A* **1999**, *153*, 551–566.

20 C. J. G. Plummer, H. H. Kausch, C. Creton, F. Kalb, L. Léger, *Macromolecules* **1998**, *31*, 6164–6176.

21 P. Rublon, B. Huneau, N. Saintier, S. Beurrot, A. Leygue, E. Verron, C. Mocuta, D. Thiaudière, D. Berghezan, *J. Synchrotron Radiat.* **2013**, *20*, 105–109.

22 N. Yan, H. Xia, Y. Zhan, G. Fei, *Macromol. Mater. Eng.* **2013**, *298*, 38–44.

23 K. Bruening, K. Schneider, S. V. Roth, G. Heinrich, *Polymer* **2013**, *54*, 6200–6205.

24 S. Trabelsi, P. A. Albouy, J. Rault, *Macromolecules* **2002**, *35*, 10054–10061.

25 J. B. Le Cam, E. Toussaint, *Macromolecules* **2010**, *43*, 4708–4714.

26 S. Mzabi, D. Berghezan, S. Roux, F. Hild, C. Creton, *J. Polym. Sci. Part B: Polym. Phys.* **2011**, *49*, 1518–1524.

27 S. Beurrot, B. Huneau, E. Verron, *J. Appl. Polym. Sci.* **2010**, *117*, 1260–1269.

28 S. Mzabi, PhD thesis, Caractérisation et analyse des mécanismes de fracture en fatigue des élastomères chargés; Université Pierre et Marie Curie: Paris, **2010**; p 304.

29 J. B. Le Cam, B. Huneau, E. Verron, L. Gornet, *Macromolecules* **2004**, *37*, 5011–5017.

30 R. Stephenson, *J. Elasticity* **1982**, *12*, 65–99.

31 R. Long, V. R. Krishnan, C.-Y. Hui, *J. Mech. Phys. Solids* **2011**, *59*, 672–695.

32 Small Angle X-ray Scattering; O. K. O. Glatter, Ed.; Academic Press: London, **1982**.

33 H. Zhang, A. K. Scholz, J. de Crevoisier, F. Vion-Loisel, G. Besnard, A. Hexemer, H. R. Brown, E. J. Kramer, C. Creton, *Macromolecules* **2012**, *45*, 1529–1543.

34 H. Zhang, A. K. Scholz, F. Vion-Loisel, Y. Merckel, M. Brieu, H. Brown, S. Roux, E. J. Kramer, C. Creton, *Macromolecules* **2013**, *46*, 900–913.

35 H. Zhang, A. K. Scholz, Y. Merckel, M. Brieu, D. Berghezan, E. J. Kramer, C. Creton, *J. Polym. Sci. Part B: Polym. Phys.* **2013**, *51*, 1125–1138.

36 J. de Crevoisier, G. Besnard, Y. Merckel, H. Zhang, F. Vion-Loisel, J. Caillard, D. Berghezan, C. Creton, J. Diani, M. Brieu, F. Hild, S. Roux, *Polym. Test.* **2012**, *31*, 663–670.

37 J. B. Le Cam, *Rubber Chem. Technol.* **2010**, *83*, 247–269.

38 J. B. Le Cam, E. Toussaint, *Mech. Mater.* **2009**, *41*, 898–901.

39 R. A. Bubeck, D. J. Buckley Jr., E. J. Kramer, H. R. Brown, *J. Mater. Sci.* **1991**, *26*, 6249–6259.

40 S. Beurrot-Borgarino, B. Huneau, E. Verron, P. Rublon, *Int. J. Fatigue* **2013**, *47*, 1–7.

41 G. A. Maier, G. Wallner, R. W. Lang, P. Fratzl, *Macromolecules* **2005**, *38*, 6099–6105.

42 T. Narayanan, *Curr. Opin. Colloid Interface Sci.* **2009**, *14*, 409–415.

43 P. J. Flory, Principles of Polymer Chemistry; Cornell University Press: Ithaca, NY, **1953**.

44 Y. Rharbi, B. Cabane, A. Vacher, M. Joanicot, F. Boue, *Europhys. Lett.* **1999**, *46*, 472–478.

45 V. R. Krishnan, C. Y. Hui, R. Long, *Langmuir* **2008**, *24*, 14245–14253.

46 K. Bruning, K. Schneider, S. V. Roth, G. Heinrich, *Macromolecules* **2012**, *45*, 7914–7919.

47 K. Brüning, K. Schneider, G. Heinrich, *J. Polym. Sci. Part B: Polym. Phys.* **2012**, *50*, 1728–1732.